Engineering Structures 349 (2026) 121837

Contents lists available at ScienceDirect

Engineering Structures

journal homepage: www.elsevier.com/locate/engstruct

Development of a novel energy fuse for enhancing blast resistance in masonry infill walls

Gholamreza Ostadi Asl [a,*], Somayeh Mollaei [a,*], Shahram Derogar [b], Fatemeh Nadiri Soflu [c], Ceren Ince [d,*], Flavio Stochino [e]

[a] Faculty member, Department of Civil Engineering, University of Bonab, Bonab, East Azerbaijan, Iran
[b] AVOVE Utilities, 183 St. Vincent Street, Glasgow G2 5QD, UK
[c] M.Sc. in Structural Engineering, Department of Civil Engineering, University of Bonab, Bonab, East Azerbaijan, Iran
[d] School of Energy, Geoscience, Infrastructure and Society, Institute for Sustainable Built Environment, Heriot-Watt University, Edinburgh, Scotland EH14 4AS, UK
[e] Department of Civil Environmental Engineering and Architecture, University of Cagliari, via Marengo 2, Cagliari, CA 09123, Italy

ARTICLE INFO

Keywords:
Blast resistance
Masonry infill wall
Energy fuse
Autoclaved aerated concrete (AAC)
Structural retrofitting

ABSTRACT

This study investigates the effectiveness of autoclaved aerated concrete (AAC) blocks as vertically embedded energy fuses for enhancing the blast resistance of masonry infill walls. A novel configuration is proposed, in which AAC layers act as sacrificial and replaceable elements that absorb and redistribute blast energy before it is transmitted through the wall. Validated finite element models were developed to simulate the structural behaviour of infill walls subjected to a wide range of explosive charge weights and standoff distances. Key response parameters, including support reactions, energy dissipation, displacement, velocity, and stress distribution in mortar, brick, and AAC components, were systematically evaluated. The results demonstrate that the AAC fuse system significantly improves blast performance: peak wall displacement was reduced by up to 80 %, base reaction forces by approximately 7 %, and peak stresses in mortar and brick by 59 % and over 30 %, respectively. Additionally, the presence of AAC layers reduced sensitivity to boundary conditions, highlighting its potential in retrofit applications where full anchorage is not feasible. The system also enhanced structural damping, promoted more uniform deformation patterns, and improved energy absorption over time relative to conventional masonry walls. These findings confirm that the proposed AAC energy fuse represents a practical and cost-effective strategy for improving the blast resilience of masonry infill walls, particularly in aging or vulnerable structures where traditional reinforcement methods may be difficult to implement.

1. Introduction

Blast events, whether accidental or intentional, represent a significant and persistent threat to urban infrastructure. Although making buildings fully blast-resistant is rarely cost-effective, significant research and practice have focused on developing mitigation strategies that reduce damage and enhance structural resilience. These include sacrificial cladding systems [1,2], fibre-reinforced overlays [3], and passive energy-dissipating devices such as dampers and base isolators [4–8]. Despite their technical potential, these systems are often associated with high implementation costs, construction complexity, or limited effectiveness under near-field or contact blast conditions [9,10]. Consequently, there remains a clear need for simple, cost-efficient, and adaptable blast mitigation approaches that can be practically integrated into conventional construction practices without requiring extensive redesign or retrofitting.

Masonry infill walls, typically constructed from clay bricks or concrete blocks, are among the most widely used non-structural components in residential, commercial, and industrial buildings worldwide [11]. Although primarily intended for thermal insulation and space division, these walls often contribute significantly to lateral load resistance in low- and mid-rise structures [1]. However, their inherently brittle behaviour, low tensile strength, and limited ductility render them highly susceptible to damage under blast-induced loading, particularly when exposed to near-field explosions [12–15]. Experimental and post-event assessments have consistently shown that such walls are

* Corresponding authors.
E-mail addresses: Ostadi@ubonab.ac.ir (G. Ostadi Asl), s.mollaei@ubonab.ac.ir (S. Mollaei), s.derogar@gmail.com (S. Derogar), fatemehnadiri7@gmail.com (F. Nadiri Soflu), C.Ince@hw.ac.uk (C. Ince), fstochino@unica.it (F. Stochino).

https://doi.org/10.1016/j.engstruct.2025.121837
Received 26 July 2025; Received in revised form 20 October 2025; Accepted 21 November 2025

prone to flexural cracking, out-of-plane displacements, and sudden collapse, even when reinforced [16,17]. These brittle failure mechanisms not only compromise structural safety but also increase the risk of secondary debris hazards, posing additional threats to occupants and adjacent structures. Furthermore, extensive damage often necessitates complete wall reconstruction, resulting in substantial repair costs and prolonged service disruption.

Considerable experimental and computational research has addressed the behaviour of masonry and autoclaved aerated concrete (AAC) walls subjected to blast and impact loading [12–15,18–22]. Blast waves typically generate a combination of flexural, shear, and localized failure modes, particularly in brittle materials [23,24]. Hao [25], using AUTODYN simulations, demonstrated brittle disintegration of unreinforced brick masonry at moderate standoff distances. Yankelevsky and Avnon [26] observed that although AAC exhibits progressive crushing and energy absorption, it remains susceptible to tensile cracking and mid-height failure under concentrated impulses. Similarly, full-scale gas explosion tests and impact studies have shown that AAC reduces debris projection and absorbs part of the blast energy, but its structural integrity is often compromised under high-intensity loads [19–22]. While these findings affirm AAC's potential as a sacrificial material, they also highlight its limitations when used as a primary load-resisting component.

Although AAC has demonstrated energy absorption capacity, its use as a monolithic or full-wall solution remains structurally inadequate under severe blast demands [12,19–22]. Studies have shown that even reinforced AAC panels experience significant deformation or fracture when exposed to high-magnitude loads [12,27,28]. Moreover, conventional blast retrofit techniques such as steel jacketing, polymer reinforcement, or fibre wraps are often intrusive, expensive, or incompatible with existing architectural constraints [3,29]. These limitations underscore the need for a blast-specific solution that can be locally integrated within masonry walls, functioning as a sacrificial buffer to absorb and dissipate energy without compromising the surrounding structure. While many retrofit systems originate from seismic applications, including FRP overlays and base isolators, their transfer to blast design contexts remains problematic. The extreme loading rate and impulsive nature of blast events challenge these systems' ability to respond effectively [3,29]. To date, AAC has not been systematically employed in a modular, wall-integrated configuration specifically designed for sacrificial energy absorption under blast loading. This research addresses that gap by proposing a targeted energy dissipation strategy that combines the energy-absorbing behaviour of AAC with a modular, wall-integrated configuration.

This study investigates the effectiveness of vertically embedded autoclaved aerated concrete (AAC) blocks, designed as sacrificial and replaceable energy fuses, for enhancing the blast resistance of masonry infill walls. The novelty of the work lies in the introduction of a modular, wall-integrated AAC fuse configuration, which differs fundamentally from previous studies that have mainly examined monolithic AAC walls or external retrofitting techniques. The proposed system provides a localized and non-intrusive energy dissipation mechanism that not only limits blast-induced damage but also facilitates post-blast reparability through selective replacement of damaged components. By reducing dependence on boundary conditions, the approach broadens applicability to both new construction and retrofit scenarios, offering a practical and adaptable solution for improving blast resilience in masonry structures. The AAC fuses are installed as non-interlocked vertical inserts, allowing any damaged units to be removed and replaced without affecting adjacent brickwork. This configuration enables practical post-event repair while maintaining the wall's overall structural integrity.

Finite element models of typical brick and block masonry walls were developed in ABAQUS/Explicit [30] to evaluate the system's effectiveness under a broad range of explosive loading conditions, both with and without AAC integration. The structural response was assessed in terms of displacement profiles, stress distribution, energy absorption, and the progression of cracking and damage, with the aim of establishing the AAC fuse as a practical and high-performance solution for blast resilience.

The proposed AAC fuse concept contributes a new direction in the blast protection of masonry infill systems by combining energy dissipation, structural modularity, and retrofit compatibility. Its localized nature allows for targeted protection without full wall replacement or excessive added mass. This makes it particularly suited to retrofit applications in aging or architecturally constrained structures, where conventional methods may be infeasible or cost prohibitive. Moreover, the potential for post-event repair through partial component replacement supports long-term resilience and lifecycle cost reduction. By demonstrating the mechanical viability and energy dissipation performance of the AAC fuse system under various blast intensities and support conditions, this research lays the groundwork for developing practical, sustainable, and structurally efficient blast mitigation strategies for both new and existing masonry construction.

2. Materials, Methods, and Modelling Approach

This section outlines the numerical framework used to evaluate the blast performance of masonry walls with and without AAC energy fuses. A series of validated finite element (FE) models were developed in ABAQUS/Explicit [30] to simulate transient responses under varying explosive loads, wall geometries, and support conditions. The modelling approach accounted for nonlinear material behaviour, strain-rate sensitivity, and damage evolution in brittle materials, enabling a realistic representation of wall response to high-intensity blast loading.

2.1. Blast Loading conditions

Only unconfined surface explosions were considered, representing realistic open-air threats to wall systems. Such loading conditions are characteristic of near-surface detonations, including vehicle-borne explosive devices, where the blast wave directly impinges on exterior walls without confinement. This approach avoids the pressure amplification and wave reflections seen in confined or internal environments [31,32]. TNT charges ranging from 5 to 2000 kg were applied at standoff distances of 2–13 m, corresponding to scaled distances (Z) between 0.9 and 7.0 m/kg$^{1/3}$. This Z-range spans near-field and far-field regimes, enabling the analysis of structural response across multiple failure modes and impulse intensities.

The Hopkinson–Cranz scaling law [33] was used to define peak overpressure, impulse, wavefront velocity, and positive phase duration as functions of charge weight and standoff distance. This law enables blast parameters to be generalised across charge sizes and geometries by using scaled distance (Z), making it widely adopted for parametric blast analysis. Several empirical models have been developed to estimate the temporal and spatial distribution of blast pressure using parameters such as scaled distance and charge mass [34–36], including peak overpressure decay, impulse duration, and pressure-time histories. Blast loads were simulated using the CONWEP module implemented in ABAQUS/Explicit [30,37]. A hemispherical surface burst configuration was assumed to reflect typical near-surface explosive scenarios on rigid ground. Gravitational loads were applied in the initial step, followed by blast pressures in a separate analysis step. This sequence ensured that the self-weight effects were stabilised before the application of transient blast loading.

2.2. Wall geometry and embedded AAC fuse system

Individual clay bricks measured 230 × 110 × 76 mm, while AAC blocks were 300 × 300 × 76 mm. Two wall configurations were modelled: a reference wall composed entirely of clay bricks, and a modified wall incorporating vertical AAC strips embedded as energy fuses. Both wall types included standard 10 mm mortar joints. The reference wall had overall dimensions of 2.87 × 2.87 m, while the AAC-integrated wall measured 3.0 × 3.5 m to accommodate the vertical AAC blocks (the fuses) along the wall height. The slight increase in wall size was necessary to ensure symmetric placement of the AAC strips and consistent spacing across the span, thereby avoiding edge effects and enhancing wave dispersion modelling. The AAC strips were placed vertically at equal spacing to act as sacrificial energy absorbers that deform through progressive crushing.

This vertical fuse arrangement was intended to disrupt blast-induced stress wave propagation and concentrate damage within controlled zones. By localising the failure region, the system enhances repairability and maintains overall wall stability, particularly under repeated or near-field blast exposure. The concept offers a lightweight, modular retrofit strategy suitable for both new and existing buildings where conventional strengthening approaches may be impractical.

Two boundary conditions were considered: fully pinned (all edges restrained) and top–bottom support only, representing traditional masonry anchorage and modern infill systems with vertical edge release. In both cases, the vertical edges of the wall were modelled as hinged supports, reflecting the partial restraint typically assumed for masonry infill systems. Fig. 1 provides detailed representations of the wall geometries (with dimensional annotations), AAC fuse placement, and boundary conditions.

2.3. Material properties and selection

In this study, the selection of an appropriate material model for AAC was guided by both experimental testing and established code-based formulations. The authors conducted laboratory tests on AAC specimens to determine key mechanical properties, including compressive strength, tensile strength, and flexural capacity. These properties provided the basis for developing calibrated constitutive relationships capable of simulating AAC's nonlinear response under dynamic blast loading. Given the brittle behaviour and strain-rate sensitivity of AAC, the model had to capture progressive crushing and stiffness degradation under high loading rates. The stress–strain behaviour of AAC in compression was defined using the relationship proposed by Entezari and Esmaili [38], as given in Eqs. (1) and (2).

$$f_c = f_c' \left[\frac{n^{pq\left(\frac{\epsilon_c}{\epsilon_0}\right)}}{\left(\frac{\epsilon_c}{\epsilon_0}\right)^{npq} + n^{pq-1}} \right] \quad (1)$$

$$q = 1.25 + 0.009 f_c' \quad (2)$$

In these equations:

- f_c is the compressive stress,
- f_c' is the compressive strength,
- ϵ_c is the strain,
- ϵ_0 is the strain at peak stress,
- n, p, and q are constants determined based on the mechanical properties of the AAC.

AAC is a lightweight, porous material, and its mechanical response was characterised using a combination of empirical expressions and experimental test results. Its low density and cellular microstructure result in distinct nonlinear behaviour under compressive and tensile loads, especially at high strain rates. The Concrete Damage Plasticity (CDP) [39] model was adopted to simulate AAC's rate-dependent, brittle response under dynamic blast loading. The CDP framework allows the inclusion of progressive damage accumulation and stiffness degradation, which are essential for replicating AAC's energy-absorbing behaviour.

The Concrete Damage Plasticity (CDP) model in ABAQUS/Explicit was adopted to simulate the nonlinear behaviour of AAC, brick, and mortar under blast loading. The model, originally proposed by Lubliner et al. [39] and later refined by others [40,41], accounts for tensile cracking and compressive crushing, with material degradation described through isotropic damage elasticity coupled with plasticity in both tension and compression. Inelastic strains govern stiffness degradation after peak stress, enabling the model to capture post-cracking and post-yield softening typical of brittle fracture under dynamic loads.

The calibrated CDP parameters used for AAC, brick, and mortar are listed in Table 1. AAC values were derived from published experimental studies [42], while brick and mortar parameters were taken from Lourenço [43]. These constants confirm that elastic–plastic behaviour

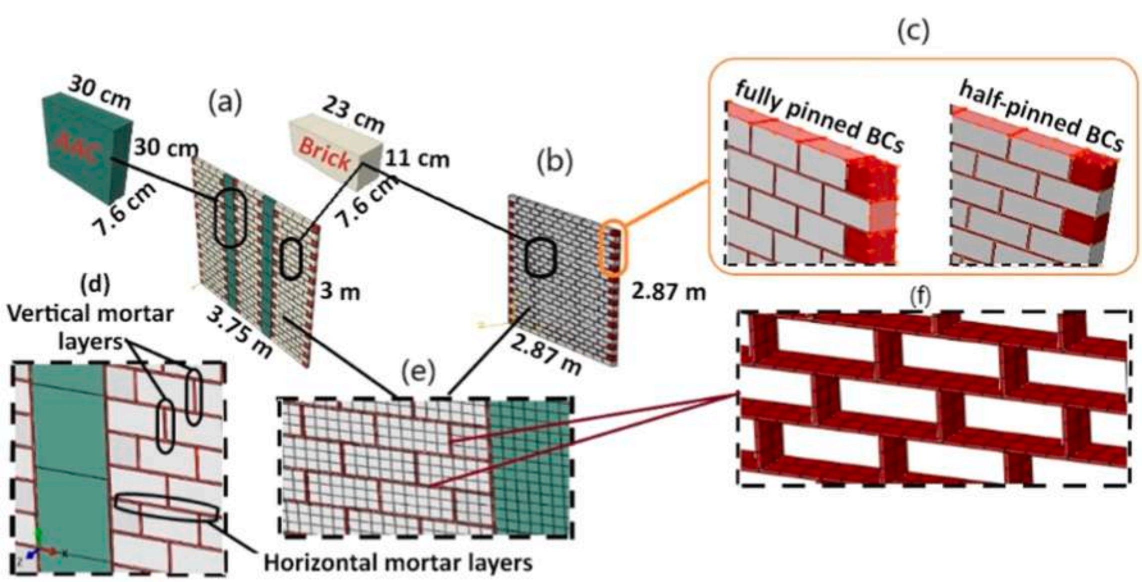

Fig. 1. Geometrical configuration and boundary conditions of the masonry infill wall with AAC fuse system: (a) AAC and brick unit dimensions; (b) reference brick wall; (c) boundary condition scenarios—fully pinned and half-pinned; (d) arrangement of vertical mortar layers showing AAC fuse inserts; (e) overall wall geometry with horizontal mortar joints; and (f) finite element meshing of the AAC-integrated wall model.

Table 1
CDP model parameters used for AAC, mortar, and brick.

Material	Dilation Angle	Eccentricity	Biaxial-to-Uniaxial Compressive Strength Ratio	Shape Factor Function	Viscoelastic Parameter
AAC	30	0.1	1.16	0.66	0.001
Mortar	15	0.1	1.16	0.66	0.0005
Brick	20	0.1	1.16	0.66	0.0005

was included for all masonry components. As the walls investigated were non-loadbearing infills subjected mainly to out-of-plane pressures, damage in mortar joints and some brick units occurred predominantly through tensile separation rather than compressive crushing.

Thermal effects were not considered, since external blast loads act within milliseconds and primarily as mechanical shock waves. In such cases, temperature rise is negligible, and no significant thermal expansion occurs. Consistent with established guidance [44,45], only the pressure and impulse components were modelled, avoiding unnecessary computational cost in the absence of reinforcement.

The elastic modulus, tensile strength, shear strength, and shear modulus were estimated based on empirical formulations recommended by the MSJC standard [46], as shown in Eqs. (3) to (6):

$$\text{Modulus of Elasticity}, E = 6500(f'_{AAC})^{0.6} \quad (\text{Mpa}), \tag{3}$$

$$\text{Tensile Strength}, \quad f_{tAAC} = 0.2\sqrt{f'_{AAC}} \quad (\text{Mpa}), \tag{4}$$

$$\text{Shear Strength}, f_v = 0.15\sqrt{f'_{AAC}} \quad (\text{Mpa}), \tag{5}$$

$$\text{Shear Modulus}, \quad E_v = 0.4 \quad E, \tag{6}$$

In the above equations, E is the modulus of elasticity, f'_{AAC} is the compressive strength of AAC materials.

Brick and mortar were modelled with densities of 1800 and 2300 kg/m^3 , elastic moduli of 9750 and 3300 MPa, and Poisson's ratios of 0.12 and 0.20, respectively. Material property definitions followed guidelines provided in the MSJC standard [46], along with empirical expressions and recommendations from previous masonry research studies [47–50]. These values were calibrated to represent typical fired clay and cementitious mortar used in non-loadbearing infill walls. A strain rate of approximately 0.03 s^{-1} was assumed for AAC under blast loading, consistent with prior experimental investigations, and was used to apply dynamic increase factors (DIFs) to all materials. DIF values ranged from 1.2 to 1.4 for compressive and tensile strength enhancements under high strain rates, as reported in prior dynamic masonry studies [51,52]. The experimentally derived compressive and tensile stress–strain behaviour of AAC and mortar used in the simulations is illustrated in Figs. 2a and 2b, respectively. The CDP model parameters adopted for AAC and mortar are summarised in Table 1, while the calibrated mechanical properties of all materials used in the FE model are listed in Table 2.

2.4. Finite element modelling

A micro-modelling approach was adopted, in which bricks, AAC blocks, and mortar layers were represented as discrete continuum components. Eight-node linear brick elements (C3D8R) were employed for all solid materials. This meshing strategy allowed localised damage, interfacial separation, and strain localisation to be captured with greater fidelity than macro-modelling approaches. The interaction surfaces between bricks, AAC blocks, and mortar joints were defined using surface-based contact, as shown in Fig. 3. Given the highly dynamic nature of blast loading, ABAQUS/Explicit [30] was selected due to its suitability for solving nonlinear, transient problems involving severe strain-rate effects and material damage evolution. Explicit time integration is particularly well suited for capturing the rapid load application and structural response of brittle components under blast conditions.

Gravity and blast loads were applied within a single Dynamic, Explicit step in ABAQUS, with the Nlgeom option activated to account for geometric nonlinearity and large deformations. The gravity load was assigned to the entire model using the LOAD module, with an amplitude ramp of 30 ms to ensure quasi-static stabilization before the blast impulse was introduced. This approach avoided artificial oscillations from instantaneous gravity application while maintaining solver consistency throughout the analysis.

The connections between bricks, AAC units, and mortar joints were defined using the general contact algorithm in the INTERACTION module. The contact surfaces were modelled with isotropic frictional behaviour combined with cohesive bonding, enabling the transfer of normal and shear stresses up to failure, after which separation and sliding were allowed. This formulation captures both adhesion and potential debonding at AAC–brick–mortar interfaces, which are critical for simulating realistic blast response.

Two boundary restraint configurations were applied to the wall models to examine the influence of edge fixity under blast loading. In the first configuration, all four edges of the wall were fully restrained

Table 2
The properties of the used materials.

	AAC	Brick	mortar
Shear damage	fracture strain: 0.004 shear stress ratio: 0.22 strain rate: 0.03	N.D.	N.D.
Density (kg/m^3)	750	1800	2300
Young's modulus (MPa)	12160	8750	13300
Poisson ratio	0.2	0.12	0.2

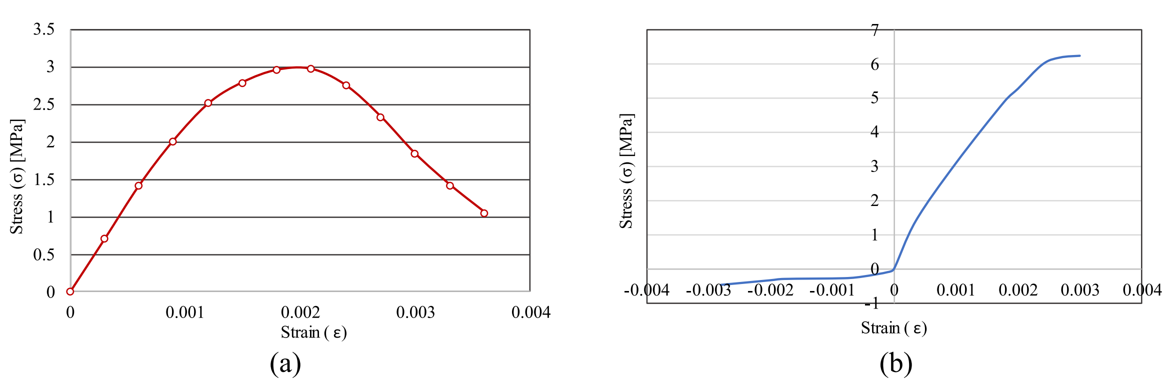

Fig. 2. Stress–strain relationships for materials used in the finite element model: (a) autoclaved aerated concrete (AAC) with a compressive strength of 3 *MPa*, (b) mortar material.

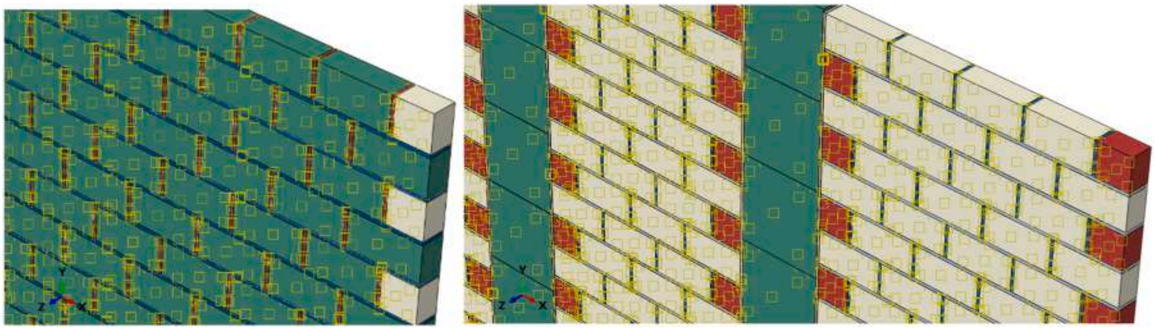

Fig. 3. Definition of interaction surfaces between masonry wall components, including bricks, AAC blocks, and mortar joints.

(pinned), representing a traditional infill condition with full frame confinement. In the second configuration, only the top and bottom edges were fixed, while the vertical sides were left free to simulate partial-restraint conditions typical of modern infill systems. No connector elements were used; the constraints were directly applied to the boundary nodes using the LOAD module in ABAQUS.

A mesh sensitivity study was performed by comparing base reaction forces and computational costs across different mesh sizes. As illustrated in Fig. 4, a 20 mm element size offered a satisfactory balance between solution accuracy and efficiency and was adopted for all subsequent simulations. This mesh was fine enough to capture strain gradients and crack development while remaining computationally feasible for large parametric runs. The validated FE models formed the basis for benchmark comparisons and systematic evaluation of the AAC fuse system across varying blast intensities and support conditions.

3. Results and discussion

3.1. Verification

To validate the developed finite element model, simulation results were compared with the benchmark study by Hao [25], which analysed a masonry wall subjected to a 2-ton TNT blast at a 13-meter standoff ($Z = 1\ m/kg^{1/3}$) using AUTODYN. ABAQUS/Explicit was adopted in this study for its proven capability to model strain rate–sensitive materials and capture nonlinear dynamic behaviour, making it suitable for blast-induced response in masonry structures.

The model closely replicated Hao's boundary conditions, geometry, and material properties. As shown in Fig. 5(a, b), the failure modes and deformation patterns from the current simulation aligned well with the reference, with minor deviations likely due to differences in solvers and mesh discretization.

Fig. 6 compares mid-span displacement and velocity histories between the two models, showing consistent trends in peak values and dynamic timing. The maximum deviation remained within 5 %, confirming the model's reliability and supporting its use for subsequent parametric analyses.

To further strengthen the verification, comparisons were also made with the experimental–numerical investigation by Yu et al. [12], which performed full-scale blast tests on AAC masonry walls. The reference wall model "116-A" was subjected to a 10,000 kg TNT explosion at a 100 m standoff distance ($Z = 4.64\ m/kg^{1/3}$). In that study, the surrounding reinforced-concrete frame remained linearly elastic; therefore, in the present model, rigid boundary constraints were applied to represent the same restraint condition while maintaining computational efficiency. As illustrated in Fig. 5(c, d), the deformation and failure patterns predicted by the present model correspond closely with both the experimental observations and the numerical results reported by Yu et al. [12], reproducing the same central cracking, block ejection, and overall wall response under blast loading. This agreement confirms the robustness of the modelling approach and reinforces confidence in its predictive capability. Although Yu et al. [12] did not publish detailed load–deformation histories for direct quantitative comparison, the close agreement in observed failure patterns provides strong qualitative validation of the finite-element model.

3.2. Reaction forces

Reaction forces were extracted in the horizontal (z) direction using the ABAQUS output variable RF3, obtained from the constrained perimeter nodes through History Output Requests defined in the Step module. This procedure provided the complete time-history of reaction forces during the blast event. Figs. 7a and 7b show the time-history of support reaction forces for walls with and without AAC energy fuses, respectively. Each scenario is labelled by charge and distance (e.g., "AAC_2000_13_RF" represents the reaction force for a wall with AAC subjected to a 2000 kg TNT explosion at a standoff distance of 13 m). As expected, peak reaction forces correlate with scaled distance (Z). For example, a 10 kg charge at 5 m and a 500 kg charge at 13 m ($Z = 2.32\ m/kg^{1/3}$) result in nearly identical peak forces (~90 kN), highlighting the consistency of blast intensity at equal Z.

AAC-integrated walls generally exhibit higher peak reaction forces

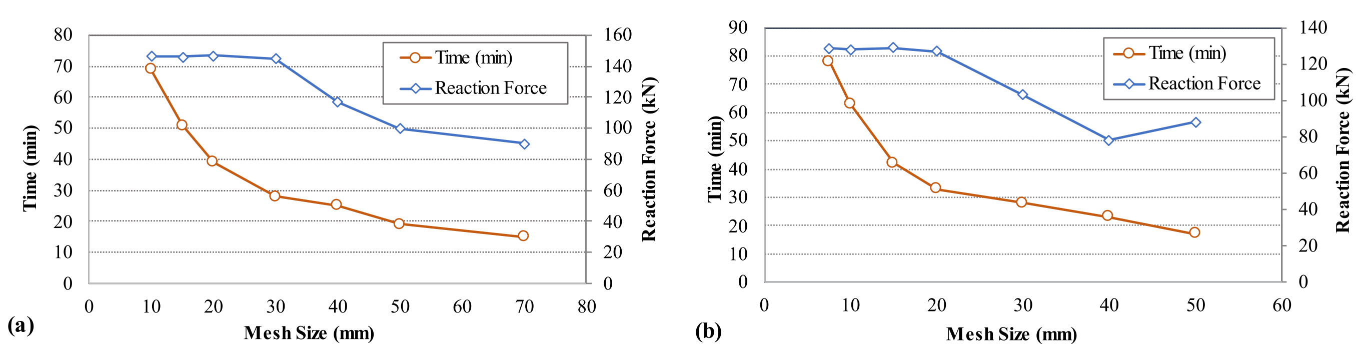

Fig. 4. Mesh sensitivity analysis results for (a) walls with AAC and (b) walls without AAC.

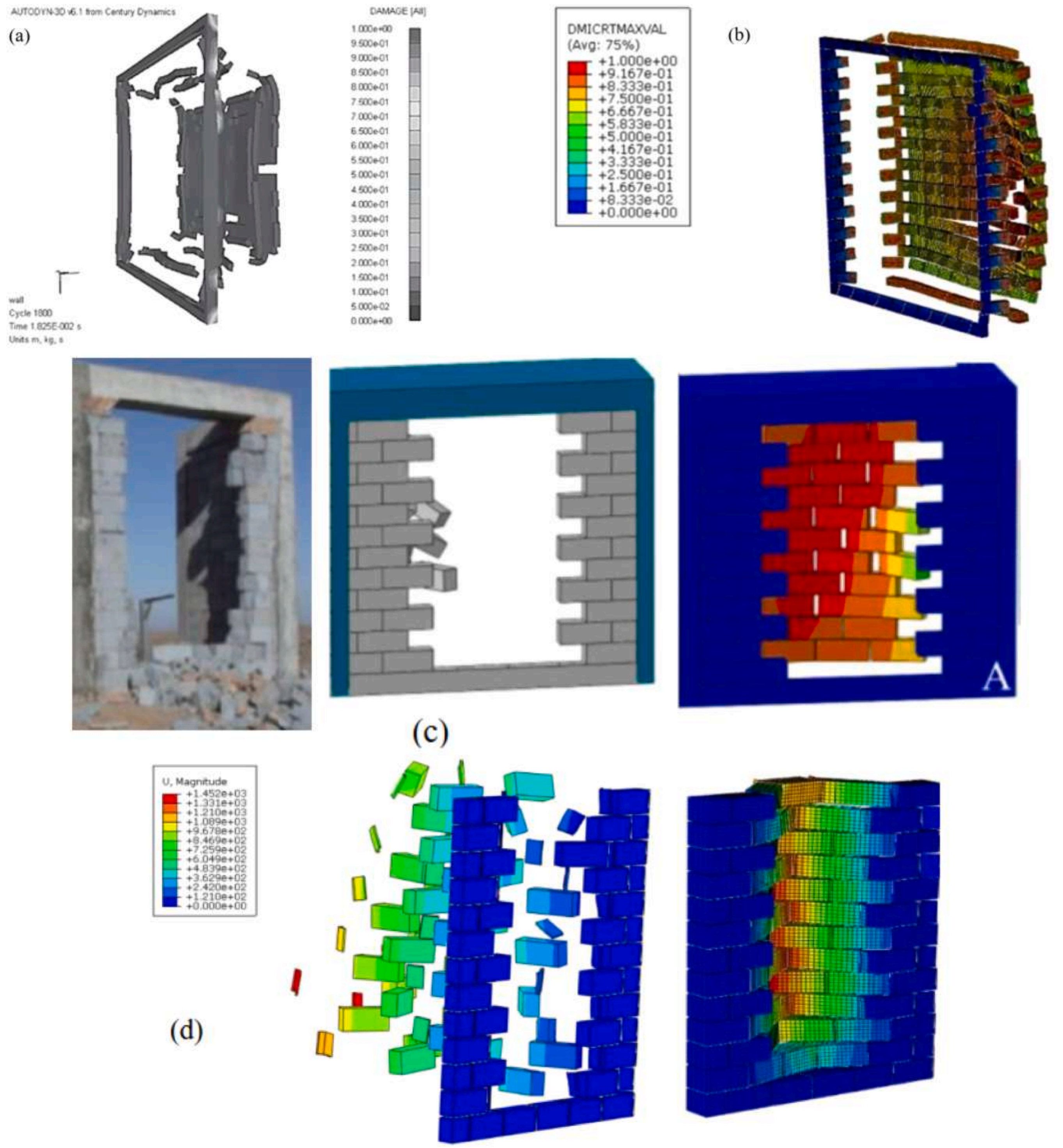

Fig. 5. Comparison of failure patterns in masonry walls subjected to blast loading: (a) reference model from Hao [25]; (b) Validation of Hao's model reproduced in this study; (c) Experimental and numerical results of wall 116-A from Yu et al. [12]; (d) Corresponding failure pattern obtained in the present FE model.

than conventional ones. While this may seem counterintuitive, it reflects the AAC wall's sustained structural engagement and integrity. Unlike conventional masonry, which tends to fail early and shed loads, AAC layers preserve continuity, enabling greater force transfer over a longer period.

As shown in Fig. 7(a), the reaction-force histories of the AAC-integrated wall exhibit smoother and more stable curves, reflecting the progressive crushing of the AAC fuses and their ability to redistribute loads over time. In contrast, Fig. 7(b) shows that the conventional wall develops sharper peaks followed by abrupt drops, corresponding to brittle cracking and rapid stiffness degradation once cracking initiates. This comparison demonstrates that the inclusion of AAC fuses enhances the damping and energy-dissipating capacity of the system while reducing the severity of transient force spikes under comparable blast intensities.

The AAC-enhanced walls also show more stable oscillatory behaviour and reduced force fluctuations, indicating improved energy redistribution and damping. These characteristics are further illustrated in

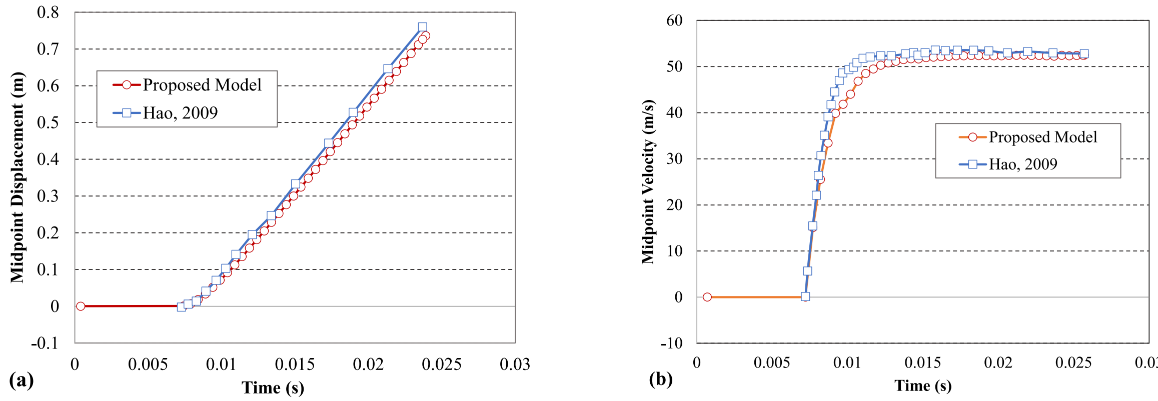

Fig. 6. Mid-point response of the masonry wall under blast loading from the present study and reference model [25]: (a) displacement; (b) velocity.

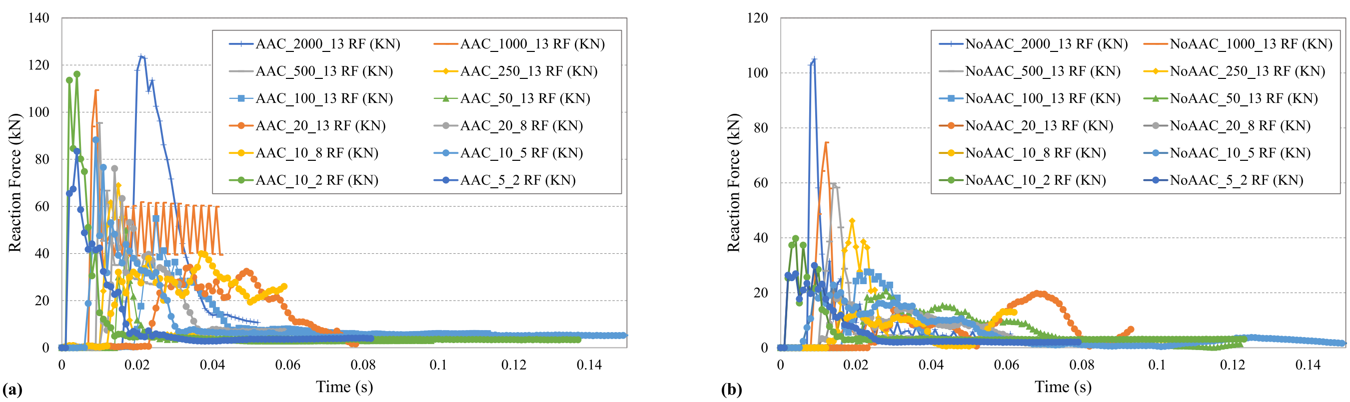

Fig. 7. Time history of the reaction force under various blast loading scenarios for the walls; (a) with AAC fuse, (b) without AAC fuse.

Fig. 8 and subsequent sections. Though AAC does not always reduce peak forces, it improves damage control and deformation uniformity, which are key for life safety and post-blast performance.

Fig. 8 provides visual comparisons of wall deformation under equivalent blasts. Under fully restrained conditions, the standard wall (8a) exhibits severe central damage, while the AAC-integrated wall (8b) shows more uniform displacement. For top-bottom supported cases, the wall without AAC (8c) suffers large out-of-plane motion, whereas the wall with AAC (8d) demonstrates improved confinement and energy dissipation.

These findings underscore the dual importance of AAC fuses and boundary conditions. While AAC integration clearly enhances damage control and energy absorption, its benefits are further amplified when combined with appropriate boundary restraints. Fully restrained walls showed better confinement, whereas simply supported walls with AAC also demonstrated significant improvement. This suggests that intentional selection of boundary conditions, alongside AAC fuse implementation, can meaningfully influence the blast resilience and efficiency of new masonry designs.

Overall, Figs. 7 and 8 confirm the effectiveness of AAC energy fuses in enhancing masonry wall performance under blast loads and establish a foundation for the following parametric study.

3.3. Absorbed energy

To quantify the energy absorption capacity of the wall systems, the total dissipated energy was obtained by summing the contributions from plastic dissipation (ALLPD), damage (ALLDMD), friction (ALLFD), and viscous dissipation (ALLVD). These parameters were extracted as history outputs for the entire FE model, and their cumulative values were integrated overall output time steps, yielding the permanently dissipated energy of the wall system under blast loading. The calculated results are summarised in Table 3, which presents the total dissipated energy for representative charge weights and standoff distances. The results demonstrate that AAC-integrated walls consistently dissipate more energy than conventional masonry walls, particularly under medium and large charge scenarios, confirming that the proposed fuse system provides a more effective mechanism for redistributing and dissipating blast energy while reducing the demand on brittle components.

Fig. 9 presents the energy dissipation profiles of wall models with and without AAC energy fuses under various blast scenarios. Each curve corresponds to a specific charge and standoff distance, using the same labelling convention as in Section 3.2. Across all cases, AAC-integrated walls demonstrate greater total energy absorption than their non-AAC counterparts. Conventional walls show an early, sharp rise in absorbed energy that plateaus quickly, indicating brittle failure and limited dissipation. In contrast, AAC-enhanced walls exhibit a more sustained energy uptake, resulting in higher cumulative dissipation.

These patterns are consistent with previous findings. As seen in Fig. 7, AAC walls show damped force responses, and Fig. 8 illustrates less localized damage and more uniform deformation. Together, these observations reinforce the role of AAC fuses in reducing dynamic effects and delaying failure via distributed energy absorption.

AAC's performance is largely attributed to its mechanical characteristics. As a lightweight, porous material, it undergoes progressive crushing under high strain rates. Unlike brittle masonry, AAC dissipates energy plastically over time. Its cellular structure also helps attenuate stress wave propagation, enhancing its mitigation capability.

Importantly, this study emphasizes the benefits of using AAC in a fuse-type layout rather than as full infill. Prior studies [3,12,14] show that fully AAC-filled walls, though capable of absorbing energy, often fail prematurely under intense blasts due to low tensile strength and

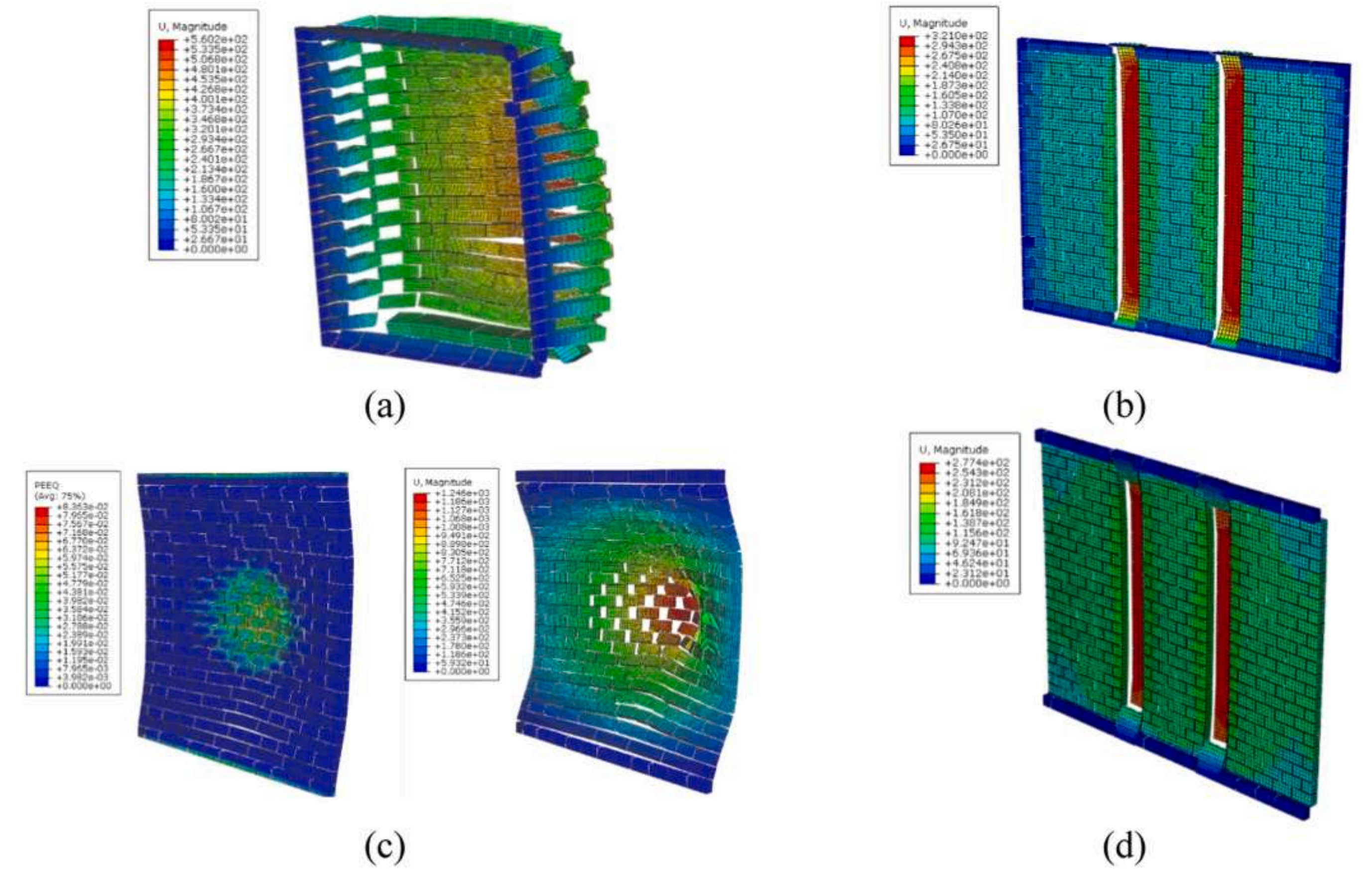

Fig. 8. Deformed shapes of masonry walls under identical blast loading conditions: (a) wall without AAC, fully restrained; (b) wall with AAC, fully restrained; (c) wall without AAC, simply supported at top and bottom; (d) wall with AAC, simply supported at top and bottom.

Table 3
Total dissipated energy of masonry wall models under different TNT charge weights and standoff distances, comparing conventional and AAC-integrated configurations (values in kJ).

TNT @ Distance	2000 Kg @ 13 m	1000 Kg @ 13 m	500 Kg @ 13 m	250 Kg @ 13 m
With AAC	10976.4	1277.8	670.4	281.2
No_AAC	5444.3	572.7	221.7	198.2
TNT @ Distance	100 Kg @ 13 m	50 Kg @ 13 m	20 Kg @ 13 m	20 Kg @ 8 m
With AAC	89.8	68.7	36.5	54.0
No_AAC	56.9	39.1	15.9	23.8
TNT @ Distance	10 Kg @ 8 m	10 Kg @ 5 m	10 Kg @ 2 m	5 Kg @ 2 m
With AAC	39.1	55.9	171.2	110.7
No_AAC	16.6	41.8	150.7	100.3

poor confinement. By embedding AAC strips vertically, the current approach uses them as sacrificial absorbers while preserving the surrounding masonry. This maintains structural integrity, improves blast resilience, and supports post-blast repairability. The fuse layout avoids the weaknesses of full infill and offers a practical and adaptable solution for blast protection.

At very close blast ranges (Figs. 9j–9l, 2 to 5m standoff), the performance gap between AAC and non-AAC walls narrows. Although AAC still absorbs more energy, the margin decreases due to limited engagement time under rapid loading. Even so, AAC fuses provide modest benefits by delaying failure onset. These results suggest AAC fuses are most effective at moderate to long standoff distances, while still offering marginal improvements in severe, near-field blasts.

3.4. Displacement response

Fig. 10 presents the time-history of midpoint displacement for masonry wall models subjected to various blast loading scenarios, comparing configurations with and without the proposed AAC energy fuse. In all cases, the incorporation of AAC layers results in a substantial reduction in displacement and a more stable dynamic response.

A representative case is shown in Fig. 10b, where a 500 kg TNT explosion at a standoff distance of 13 m causes a peak displacement exceeding 180 mm in the wall without AAC, indicating severe out-of-plane deformation and potential instability. In contrast, the wall equipped with the AAC fuse limits displacement to approximately 26 mm, clearly demonstrating the effectiveness of the energy-absorbing mechanism in mitigating structural motion. Similar trends are observed in Figs. 10c to 10g. For instance, under a 50 kg TNT load at 13 m (Fig. 10c), the wall without AAC reaches a peak displacement of approximately 300 mm, which represents extreme deformation likely to exceed acceptable structural performance limits. In contrast, the AAC-integrated wall limits the movement to around 52 mm, highlighting a substantial improvement in blast resilience.

In addition to peak displacement magnitudes, the time-dependent response curves offer insight into post-blast deformation stability and indicate differences in recovery behaviour between the AAC and non-AAC configurations. Non-AAC walls often exhibit continuously increasing displacement over time, reflecting progressive plastic deformation and loss of stiffness. In contrast, AAC-integrated walls consistently demonstrate more stable, bounded displacement profiles, with some cases showing partial rebound. This behaviour suggests improved energy dissipation and reduced residual deformation due to the buffering effect of the AAC layer.

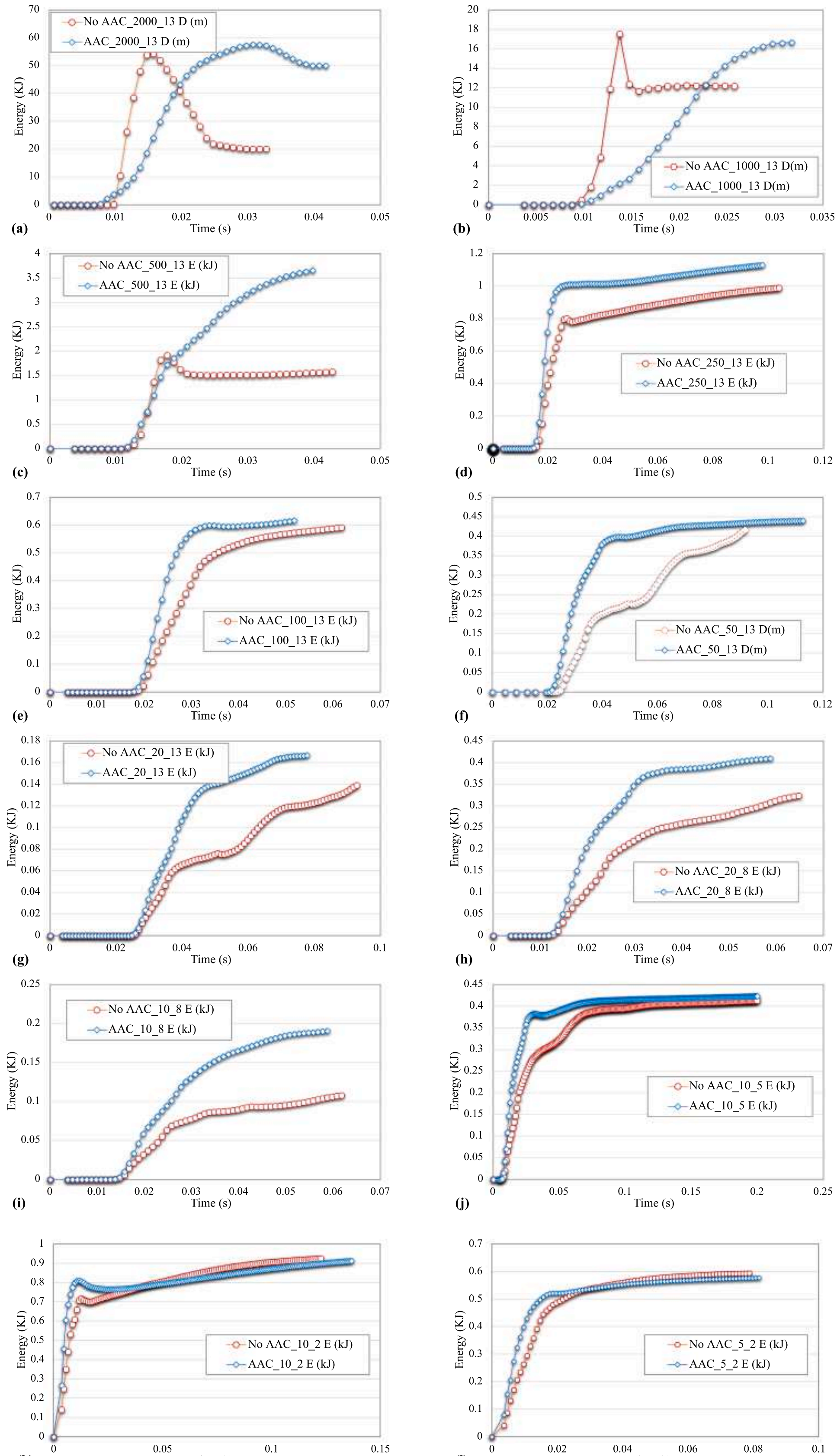

Fig. 9. Energy dissipation curves of the wall under various blast scenarios: (a) 2000 kg @ 13 m; (b) 1000 kg @ 13 m; (c) 500 kg @ 13 m; (d) 250 kg @ 13 m; (e) 100 kg @ 13 m; (f) 50 kg @ 13 m; (g) 20 kg @ 13 m; (h) 20 kg @ 8 m; (i) 10 kg @ 8 m; (j) 10 kg @ 5 m; (k) 10 kg @ 2 m; (l) 5 kg @ 2 m.

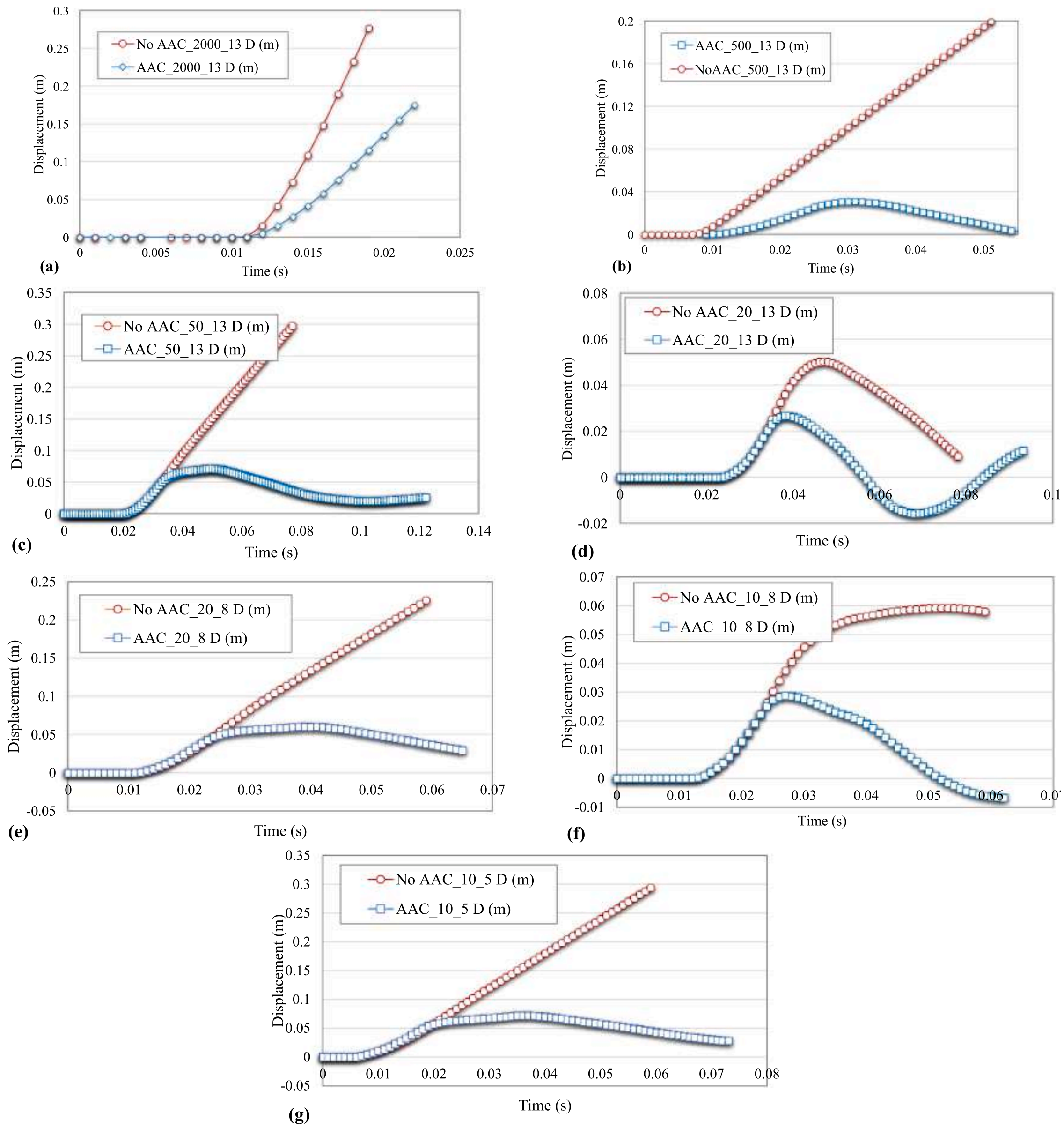

Fig. 10. Displacement time-history at the midpoint of the wall under various blast scenarios: (a) 2000 kg @ 13 m; (b) 500 kg @ 13 m; (c) 50 kg @ 13 m; (d) 20 kg @ 13 m; (e) 20 kg @ 8 m; (f) 10 kg @ 8 m; (g) 10 kg @ 5 m.

The superior performance of AAC-enhanced walls can be attributed to the progressive crushing behaviour of autoclaved aerated concrete, which absorbs energy early in the blast event. This sacrificial mechanism helps attenuate the impulse before it propagates through the wall, thereby limiting both local and global damage. Moreover, the AAC fuse can be designed as a modular and replaceable component, supporting easier post-blast repair while preserving the integrity of the primary wall system.

Overall, the findings confirm that the AAC energy fuse system provides a practical and effective strategy for mitigating blast-induced damage by significantly reducing out-of-plane displacements across a wide range of realistic explosive threats. In addition to displacement reductions, analysis of plastic-strain distribution showed that the clay brick units and most mortar joints did not undergo significant plastic deformation, as their behaviour was dominated by tensile cracking and interfacial separation. In contrast, the AAC components developed localised plastic strains due to progressive crushing, thereby confirming their intended role as sacrificial energy-absorbing fuses.

3.5. Velocity response

Fig. 11 presents the time-history of midpoint velocity in masonry wall models subjected to various blast loading scenarios, comparing the dynamic response of walls with and without the AAC energy fuse. In all examined cases, the inclusion of AAC layers results in a reduction in peak velocity and a more controlled post-peak behaviour, highlighting the role of the AAC fuse in moderating blast-induced motion.

For instance, under a 2000 kg TNT blast at a standoff distance of 13 m (Fig. 11a), the non-AAC wall reaches a peak velocity of approximately 12.3 m/s, with the velocity profile remaining nearly flat afterward. In contrast, the AAC-integrated wall reaches a lower peak of about 10.5 m/s and then gradually declines, indicating more effective energy dissipation and damping.

A similar trend is observed under the 1000 kg TNT scenario (Fig. 11b), where the non-AAC wall peaks at approximately 7.9 m/s, while the AAC wall reaches about 5.6 m/s, representing a reduction of nearly 28 %. Additionally, the AAC wall shows a distinct post-peak

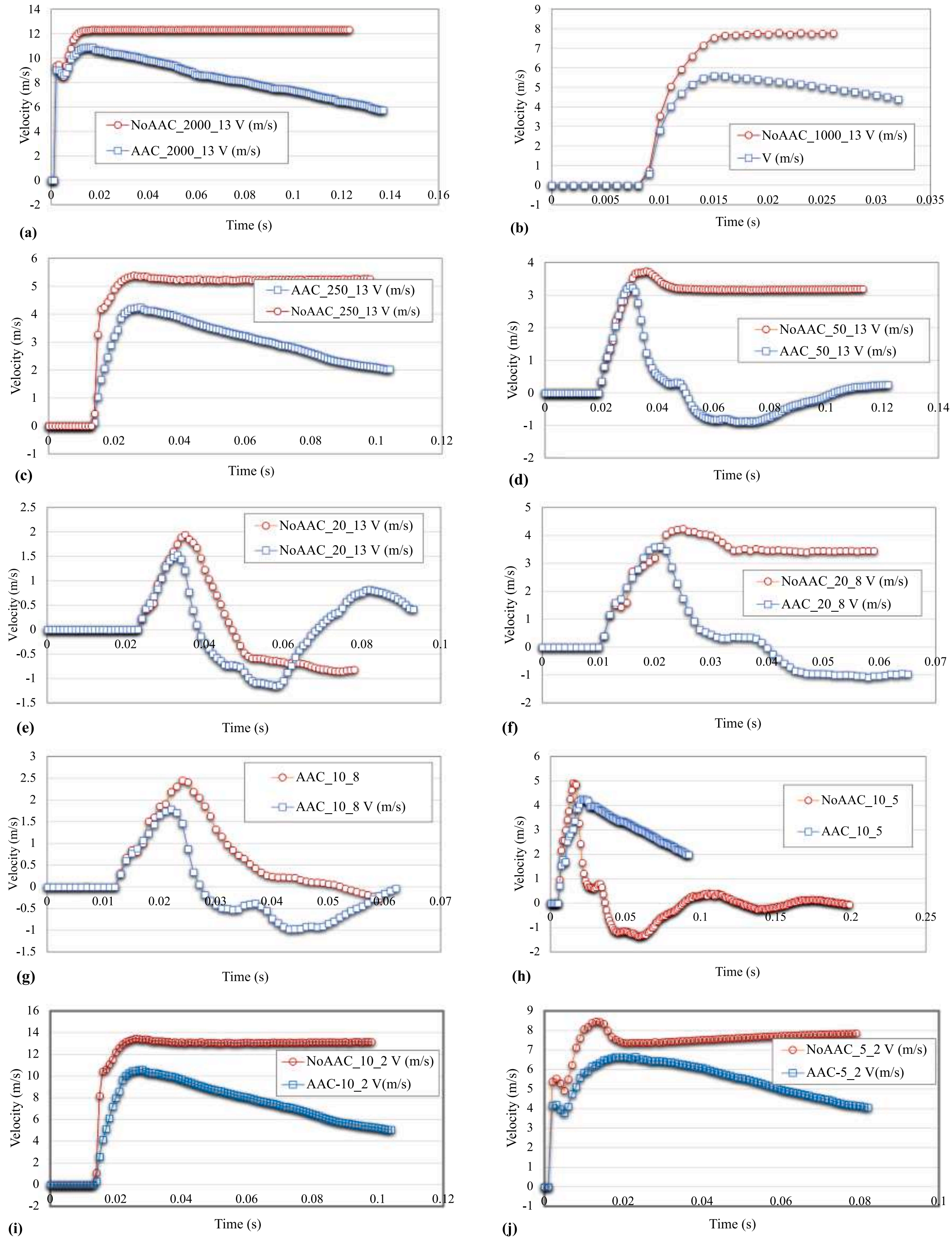

Fig. 11. Velocity time-history at the midpoint of the wall under various blast scenarios: (a) 2000 kg @ 13 m; (b) 1000 kg @ 13 m; (c) 250 kg @ 13 m; (d) 50 kg @ 13 m; (e) 20 kg @ 13 m; (f) 20 kg @ 8 m; (g) 10 kg @ 8 m; (h) 10 kg @ 5 m; (I) 10 kg @ 2 m; (i) 5 kg @ 2 m.

decay in velocity, while the non-AAC wall maintains a sustained velocity plateau, indicating less effective damping.

Other scenarios, such as the 250 kg and 50 kg TNT explosions at 13 m (Figs. 11c and 11d), further confirm this pattern. In each case, AAC-integrated walls show reduced peak velocities and transitions that are more gradual compared to the sharp rises and sustained high velocities in non-AAC walls. These patterns suggest that the AAC layers contribute to progressive energy absorption and improved dynamic stability.

In several intermediate-range scenarios (Figs. 11f to 11h), the AAC walls not only demonstrate lower peak velocities but also reach a stabilized state more quickly. Their velocity curves show smooth, monotonic decay, whereas non-AAC walls exhibit extended oscillations or abrupt fluctuations, characteristics of brittle dynamic behaviour and lower energy dissipation capacity.

Even under the closest-range blast scenarios, specifically 10 kg and

5 kg TNT detonations at a 2-meter standoff (Figs. 11i and 11j), AAC-integrated walls continue to provide meaningful reductions in peak velocity. In Fig. 11i, the peak velocity drops from approximately 14.3 m/s in the non-AAC wall to 11.0 m/s with AAC, while in Fig. 11j, it decreases from 8.3 m/s to 6.5 m/s, corresponding to a reduction of roughly 23 % in both cases. These reductions are accompanied by smoother post-peak decay curves, in contrast to the plateauing or fluctuating responses seen in non-AAC walls. The consistent velocity mitigation across all blast intensities confirms that the AAC fuse mechanism remains effective even under highly impulsive loads, aligning well with trends observed in the energy absorption data.

Overall, the AAC fuse's ability to reduce peak velocities, promote smoother deceleration, and stabilize the wall's motion supports its role in mitigating blast effects. These dynamic benefits are critical for reducing the risk of flying debris, limiting structural damage, and preserving post-blast integrity.

3.6. Stress distribution

Fig. 12 presents the stress distribution histories in the wall components under a 2000 kg TNT charge at a standoff distance of 13 m ($Z = 1.03\ m/kg^{1/3}$). As shown in Fig. 12a, the maximum stress in the mortar of the wall without AAC reaches approximately 6.15 MPa, whereas the mortar in the AAC-integrated wall peaks at around 3.8 MPa. This indicates a clear stress reduction in the presence of the AAC energy fuse, highlighting its ability to alleviate force transmission to brittle mortar joints.

In the brick units (Fig. 12b), a similar trend is evident. The wall without AAC exhibits a sharp stress spike of 9.3 MPa, while the AAC-integrated wall peaks more gradually at around 6.5 MPa, indicating more uniform stress distribution. The AAC layer itself (Fig. 12c) reaches a peak of approximately 2.7 MPa, followed by a steady decline and fluctuations between 0.5 and 1 MPa. This response suggests that the AAC acts as a sacrificial element, progressively crushing to absorb blast energy and reduce stress transmitted to surrounding brick and mortar

These results align with earlier findings on energy dissipation (Fig. 9) and displacement (Fig. 10), where AAC-integrated walls showed more stable, damped responses under blast loads. Lower stress levels in mortar and brick suggest delayed crack initiation and reduced failure potential, supporting post-blast reparability. Importantly, localized stress within the AAC fuse confirms its sacrificial role. By absorbing energy early and redistributing it gradually, the AAC prevents brittle components like brick and mortar from experiencing sharp, damaging peaks, thereby improving wall resilience and structural integrity under repeated or extreme conditions.

Table 4 presents the maximum stress values in mortar, brick, and AAC components under various blast scenarios and two support conditions: fully pinned and half pinned. The results confirm that the AAC energy fuse consistently mitigates stress concentrations, especially in brittle masonry, regardless of restraint. For instance, under a 1000 kg TNT blast at a 13-meter standoff, mortar stress drops from 4.81 MPa to 1.96 MPa, and brick stress from 8.11 MPa to 5.59 MPa. These reductions demonstrate the AAC's capacity to absorb and dissipate energy before it reaches surrounding brittle materials.

It is noteworthy that the AAC components consistently remained within safe stress limits across all analysed scenarios. Peak stress values in the AAC did not exceed 3 MPa, demonstrating the material's capacity to absorb blast energy through progressive crushing. This energy-absorbing behaviour effectively reduces the transmission of high stress to adjacent brittle components, such as mortar and brick, thereby facilitating a controlled and localized dissipation of energy within the wall system.

In contrast to AAC-integrated walls, masonry walls without the fuse layer exhibit consistently higher peak stresses in both mortar and brick components, regardless of support condition. Although the difference in stress values between fully and half-pinned cases is numerically small, the absence of a dedicated energy-dissipating mechanism renders non-AAC walls more susceptible to localized damage and brittle failure. Thus, comparable peak stress magnitudes across support conditions should not be interpreted as evidence of structural robustness, but rather as a limitation in the wall's capacity to redistribute and dissipate blast energy.

To provide a quantitative evaluation of the AAC energy fuse system's effectiveness, the Stress Suppression Efficiency (SSE) was calculated for representative cases. SSE quantifies the percentage reduction in peak stress resulting from AAC inclusion, using the following relation:

$$SSE(\%) = \frac{\sigma_{No-AAC} - \sigma_{AAC}}{\sigma_{No-AAC}} \times 100 \quad (8)$$

where σ_{No-AAC} and σ_{AAC} denote the peak stress values recorded in masonry components without and with AAC integration, respectively.

Under fully pinned conditions, SSE calculations show that mortar

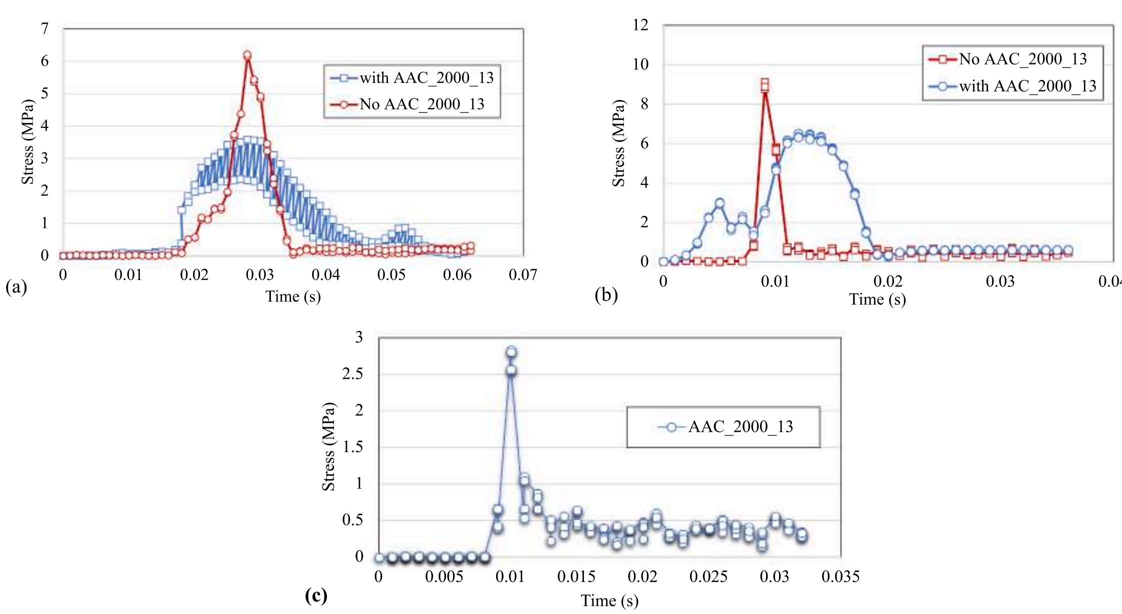

Fig. 12. Stress distribution changes under a 2000 kg-TNT charge at a standoff distance of 13 m at: a) mortar; b) brick; c) AAC.

Table 4
Maximum stress in mortar under various blast loading scenarios for two support conditions.

Feature	AAC	No_AAC	AAC	No_AAC	AAC	No_AAC	AAC	No_AAC	AAC	No_AAC	AAC	No_AAC
Mortar elements												
TNT @ Distance	2000 Kg @ 13 m		1000 Kg @ 13 m		500 Kg @ 13 m		250 Kg @ 13 m		100 Kg @ 13 m		50 Kg @ 13 m	
Max Stress (MPa) All Pinned	3.54	6.10	1.96	4.81	1.54	4.32	1.23	3.82	0.92	2.53	0.41	1.24
Max Stress (MPa) Half Pinned	3.35	6.25	2.12	5.03	1.67	4.38	1.19	3.77	0.89	2.41	0.50	1.61
TNT @ Distance	20 Kg @ 13 m		20 Kg @ 8 m		10 Kg @ 8 m		10 Kg @ 5 m		10 Kg @ 2 m		5 Kg @ 2 m	
Max Stress (MPa) All Pinned	0.21	0.92	0.47	1.81	0.39	1.26	0.81	2.86	3.62	6.13	3.08	5.75
Max Stress (MPa) Half Pinned	0.32	1.01	0.67	2.03	0.41	1.30	0.95	3.02	4.01	6.20	2.99	5.61
Brick elements												
Max Stress (MPa) All Pinned	6.29	8.90	5.59	8.11	5.31	7.96	5.27	7.90	4.42	6.24	2.97	5.11
Max Stress (MPa) Half Pinned	6.17	8.72	5.86	8.28	5.40	8.03	5.02	7.82	4.31	6.18	3.21	5.36
TNT @ Distance	20 Kg @ 13 m		20 Kg @ 8 m		10 Kg @ 8 m		10 Kg @ 5 m		10 Kg @ 2 m		5 Kg @ 2 m	
Max Stress (MPa) All Pinned	2.08	4.07	3.13	5.58	2.40	4.63	4.08	7.31	5.84	8.29	6.21	8.90
Max Stress (MPa) Half Pinned	2.17	4.12	3.87	5.84	2.75	4.90	4.61	7.44	6.33	8.91	6.07	8.65
AAC elements												
TNT @ Distance	2000 Kg @ 13 m	1000Kg@13 m	500 Kg @ 13 m	250Kg@13 m	100 Kg @ 13 m	50Kg@13 m	20Kg @ 13 m	20Kg@8 m	10 Kg @ 8 m	10Kg@5 m	10Kg @ 2 m	5Kg@2 m
Max Stress (MPa) All Pinned	2.8	2.49	2.46	2.37	2.46	2.01	1.97	1.84	1.98	1.93	2.53	2.05
Max Stress (MPa) Half Pinned	2.46	2.79	2.48	2.11	3.25	2.67	2.64	2.63	1.98	2.08	3.04	1.97

stress was reduced by approximately 59 %, while brick stress was suppressed by just over 30 %. Even in half-pinned configurations, which reflect reduced anchorage, mortar SSE remained near 50 % across all cases, while brick SSE consistently ranged from 20 % to 30 %. These reductions demonstrate the AAC fuse's consistent stress mitigation performance under both ideal and limited support conditions, reinforcing its applicability to retrofit strategies and blast-resistant masonry systems.

The improved stress behaviour is a direct consequence of the sacrificial, energy-dissipative properties of AAC. Its porous microstructure and low stiffness enable progressive crushing under high strain rates, thereby reducing the transmission of stress waves into surrounding brittle elements. This behaviour mitigates peak stress concentrations and facilitates a more uniform load distribution across the wall section.

Finally, beyond its mechanical advantages, AAC also offers notable sustainability benefits. It is lightweight, recyclable, thermally efficient, and low in embodied energy. Its ease of installation, potential for post-damage replacement, and compatibility with both new and existing construction position it as a practical and environmentally responsible solution for enhancing blast resilience in masonry structures.

3.7. Extended discussion

The results confirm that the proposed AAC fuse system markedly enhances the blast resilience of masonry infill walls. Compared with conventional walls, AAC-integrated systems dissipate more energy, reduce peak displacements, and maintain greater post-blast stability across various charge weights and boundary conditions. These improvements arise from the progressive crushing of AAC blocks, whose porous microstructure and low stiffness enable controlled energy absorption and delay the transfer of high-intensity stresses to surrounding brittle components. This sacrificial behaviour limits both local and global damage, preserving overall wall integrity and minimising debris generation.

Analysis of the residual deformation profiles indicated that the AAC-integrated walls experienced markedly smaller permanent displacements than the reference masonry walls. The improved recoverability of the AAC-integrated configuration demonstrates that the proposed fuse system successfully mitigates irreversible deformation by localising energy absorption within the AAC elements and reducing the residual demand on the surrounding masonry.

The influence of boundary conditions was also evident: fully restrained edges produced higher reaction forces, whereas half-pinned supports highlighted the AAC fuse's progressive role in redistributing loads and reducing peak stresses. While conventional infills rely heavily on perimeter restraint to resist blast loading, AAC-integrated walls maintained their protective function even under limited anchorage. This reduced dependence on edge restraint is particularly advantageous for retrofitting existing structures or designing new walls with separation joints to accommodate drift. Such performance aligns with the objectives of accidental-action provisions in BS EN 1991–1–7 [53] and the guidance for blast-resilient buildings provided in SCI Publication P244 [54].

Quantitative analysis using the Stress Suppression Efficiency (SSE) parameter confirmed the AAC fuse's capacity to mitigate stresses effectively. Mortar SSE values commonly exceeded 50 %, with peaks approaching 60 %, while brick SSE ranged between 20 % and 30 %. This demonstrates that the AAC layer acts as an early-stage energy dissipater, engaging before critical stress thresholds are reached and thereby buffering the wall response against brittle cracking or collapse.

From a practical and sustainability perspective, the AAC fuse system also offers important advantages. AAC is lightweight, recyclable, thermally efficient, and widely available, providing a low-carbon alternative to conventional blast-resistant materials. Its modular configuration enables selective replacement of damaged fuses, reducing post-event repair costs and downtime. Although this replaceability was not experimentally verified in the present study, it derives from the constructional arrangement of the AAC fuse system, which allows individual elements to be removed and substituted after a blast event.

These combined mechanical and practical benefits make AAC fuses a promising solution for both new construction and retrofit applications, especially where weight, cost, or architectural constraints limit the use of traditional strengthening methods.

4. Conclusion

This study introduced a novel energy fuse concept for blast-resistant masonry infill walls, employing vertically embedded layers of autoclaved aerated concrete (AAC) blocks. Acting as sacrificial components that can be replaced if damaged, the AAC layers serve to dissipate incoming blast energy prior to its transmission through the wall, thereby reducing both direct overpressure-induced damage and the risk of secondary fragmentation.

Acting as sacrificial components that can be replaced if damaged, the AAC layers serve to dissipate incoming blast energy prior to its transmission through the wall

A validated finite element model was developed to examine the performance of masonry walls with and without AAC integration under a wide range of blast loading scenarios. The structural responses, including displacement, velocity, reaction forces, stress distribution, and energy absorption, were systematically evaluated. The key findings are summarized as follows:

- The AAC fuse system resulted in an average reduction of approximately 7 % in base reactions, an increase of around 8 % in total absorbed energy, and up to 80 % reduction in peak wall displacement. At the material level, the incorporation of AAC layers led to peak mortar stress reductions of approximately 59 % and brick stress reductions of over 30 % under fully restrained conditions.
- While a slight increase in peak velocity was observed in a few close-range cases, AAC-integrated walls generally exhibited lower peak velocities and consistently more stable, damped responses. This behaviour reflects improved energy redistribution and reduced vulnerability to brittle failure.
- While conventional masonry walls exhibited minimal variation between support conditions, AAC-integrated walls consistently maintained their protective performance under both fully pinned and partially restrained configurations. This robustness highlights the system's applicability to retrofit scenarios and new construction where full anchorage may be impractical due to architectural constraints or seismic design requirements.
- Stress Suppression Efficiency (SSE) calculations confirmed the consistent contribution of the AAC fuse to blast-induced stress mitigation across various loading scenarios and support conditions.

Beyond structural performance, the AAC energy fuse system offers significant sustainability benefits. AAC is lightweight, thermally efficient, recyclable, and easily replaceable, making it particularly suitable for application in urban or aging buildings where architectural constraints may limit the use of conventional blast-resistant systems.

While the numerical results in this study provide validated insights into AAC-integrated wall behaviour under blast loading, further research should extend these findings through full-scale experimental testing. Additional investigations into façade configurations, the presence of openings, and multi-hazard interactions will further inform the development of low-cost, modular, energy-dissipative retrofit systems for masonry structures.

In addition to full-scale model validation, further analytical investigations are recommended to extend the applicability of the proposed system. Future work should focus on developing adaptive material models for AAC blocks that account for high strain-rate effects, as well as conducting parametric studies on the thickness of AAC units, the overall wall thickness including loadbearing configurations, and the role of vertical ties surrounding the proposed AAC fuses. Experimental verification should also address the replaceability aspect of the AAC fuses and assess the practicality of their post-event replacement procedure. These directions will help refine the predictive capability of the models and broaden the range of practical applications.

CRediT authorship contribution statement

Flavio Stochino: Methodology, Conceptualization, Writing – review & editing. **Fatemeh Nadiri Soflou:** Validation, Software, Investigation, Formal analysis. **Ceren Ince:** Writing – review & editing, Writing – original draft, Visualization, Methodology, Conceptualization. **Gholamreza Ostadi Asl:** Visualization, Supervision, Software, Project administration, Methodology. **Shahram Derogar:** Writing – review & editing, Writing – original draft, Visualization, Validation, Methodology, Investigation, Formal analysis, Conceptualization, Data curation. **Somayeh Mollaei:** Visualization, Validation, Supervision, Software, Methodology, Formal analysis, Conceptualization, Data curation, Writing – review & editing.

Declaration of Generative AI and AI-assisted technologies in the writing process

During the preparation of this work, the authors used ChatGPT by OpenAI to assist with improving the clarity, academic tone, and consistency of the manuscript's language. After using this tool, the author reviewed and edited the content as needed and takes full responsibility for the content of the publication.

Declaration of Competing Interest

The authors declare that they have no known competing financial interests or personal relationships that could have appeared to influence the work reported in this paper.

Data Availability

The data that has been used is confidential.

References

[1] Codina R, Ambrosini D, de Borbón F. New sacrificial cladding system for the reduction of blast damage in reinforced concrete structures. Int J Prot Struct 2017;8(2):221–36. https://doi.org/10.1177/2041419617701571.

[2] Zhou H, Zhang X, Wang X, Du X, Yu S, Wang Y, Jiang J. Protection effectiveness of sacrificial cladding for near-field blast mitigation. Int J Impact Eng 2022;170:e104361. https://doi.org/10.1016/j.ijimpeng.2022.104361.

[3] Badshah E, Naseer A, Ashraf M, Ahmad T. Response of masonry systems against blast loading. Def Technol 2021;17(4):1326–37. https://doi.org/10.1016/j.dt.2020.07.003.

[4] Zhang R, Phillips BM. Performance and protection of base-isolated structures under blast loading. J Eng Mech 2016;142(1). 04015063.

[5] Mohebbi M, Dadkhah HD. Performance of semi-active base isolation systems under external explosion. Int J Struct Stab Dyn 2017;17(10):1750112.

[6] Kangda MZ, Bakre S. Positive-phase blast effects on base-isolated structures. Arab J Sci Eng 2019;44:4971–92.

[7] Fang X, Bi K, Hao H, Hao D, Lie W, Chen Z, Yang X. Seismic performance enhancement of shear wall structures using lead viscoelastic coupling beam. Eng Struct 2025;332:120054. https://doi.org/10.1016/j.engstruct.2025.120054.

[8] Xiaojun F, Kaiming B, Hong H, Hao D, Wenchen L, Zhangyan C, Xiaoqiang Y. Seismic performance enhancement of shear wall structures using lead viscoelastic coupling beam. Eng Struct 2025;332:e120054. https://doi.org/10.1016/j.engstruct.2025.120054.

[9] Moradi M, Tavakoli H. Energy Balance on Steel Structure with Pall Damper under Blast Loading. Amirkabir J Civ Eng 2020;52(10):2415–34.

[10] Tavakoli H, moradi M, kiandoust M. Evaluation of the performance of a 10 story steel structure with Base Isolation under blast loads. J Struct Constr Eng 2021;8(7):214–35. https://doi.org/10.22065/jsce.2020.185505.1860.

[11] Bhaskar JK, Bhunia D, Karthik J, Samadhiya A. A state-of-the-art review on the evolution of performance of masonry infill walls under lateral loadings. Asian J Civ Eng 2022;23(7):973–1028.

[12] Yu Q, Zeng D, Xu X, Li S, Dong W, Dai L. Experimental and numerical investigation of polymer-reinforced and normal autoclaved aerated concrete masonry walls under large TNT explosive loads. Int J Impact Eng 2022;164:104188.
[13] Bayat A, Liaghat GH, Ghalami-Choobar M, Ashkezari GD, Sabouri H. Analytical modeling of the high-velocity impact of autoclaved aerated concrete (AAC) blocks and some experimental results. Int J Mech Sci 2019;159:315–24.
[14] Mollaei S, Babaei Ghazijahani R, Noroozinejad Farsangi E, Jahani D. Investigation of behavior of masonry walls constructed with autoclaved aerated concrete blocks under blast loading. Appl Sci 2022;12(17):8725.
[15] Xu WX, Bao Q, Li Z, Fan JY. Numerical Analysis on the Behavior of Autoclaved Aerated Concrete Block Infilled Wall Subjected to Gas Explosion. Appl Mech Mater 2015;723:259–65.
[16] Thango SG, Stavroulakis GE, Drosopoulos GA. Investigation of the Failure Response of Masonry Walls Subjected to Blast Loading Using Nonlinear Finite Element Analysis. Computation 2023;11(8):165. https://doi.org/10.3390/computation11080165.
[17] National Concrete Masonry Association. Design of Concrete Masonry Walls for Blast Loading. TEK 14-21A. 2013. 〈https://www.masonryandhardscapes.org/resource/tek-14-21a/〉.
[18] B. Qadir, Critical impact energy for local impact damage of hard projectile on concrete slab, 2012.
[19] Sekar T, Ramaswamy S. Performance of strengthened brick masonry under pyrotechnic explosive loading–An experimental study. Int J Appl Eng Res 2010;5(9):1491–505.
[20] Li Z, Chen L, Fang Q, Chen W, Hao H, Zhang Y. Experimental and numerical study of basalt fiber reinforced polymer strip strengthened autoclaved aerated concrete masonry walls under vented gas explosions. Eng Struct 2017;152:901–19.
[21] Li Z, et al. Study of autoclaved aerated concrete masonry walls under vented gas explosions. Eng Struct 2017;141:444–60.
[22] Hussein, A. (2019). Performance assessment of simple blast wall systems (Doctoral dissertation, Colorado State University).
[23] Hao H, Hao Y, Li J, Chen W. Review of the current practices in blast-resistant analysis and design of concrete structures. Adv Struct Eng 2016;19(8):1193–223.
[24] Zineddin M, Krauthammer T. Dynamic response and behavior of reinforced concrete slabs under impact loading. Int J Impact Eng 2007;34(9):1517–34.
[25] Hao H. Numerical modelling of masonry wall response to blast loads. Aust J Struct Eng 2009;10(1):37–52.
[26] Yankelevsky DZ, Avnon I. Autoclaved aerated concrete behavior under explosive action. Constr Build Mater 1998;12(6-7):359–64.
[27] Liu C, Liu S, Hao Y, Wu H, Wei J, Huang Y. Field testing of blast responses and strengthening methods of reinforced autoclaved aerated concrete panels. Eng Struct 2023;290:116377.
[28] Liu C, Hou J, Hao Y, Hao H, Meng X. Effect of high strain rate and confinement on the compressive properties of autoclaved aerated concrete. Int J Impact Eng 2021;156:103943.
[29] Furtado A, Rodrigues H, Arêde A, Varum H. Experimental tests on strengthening strategies for masonry infill walls: A literature review. Constr Build Mater 2020;263:120520.
[30] Abaqus v. 6.14 Documentation; Dassault Systemes Simulia Corporation: Providence, RI, USA, 2011.
[31] W. Baker, Explosions in air university of texas press, Austin and London, 1973.
[32] Yan D, Wu Q, Li T, Ren Y. Investigation and Analysis on the Explosion Accident in the Mountain Tunnel. J Eng Sci Technol Rev 2019;12(4).
[33] Cormie D, Mays G, Smith P. Blast effects on buildings. 2nd ed. Thomas Telford Publishing; 2009.
[34] Gurney RW. The initial velocities of fragments from bombs, shell, grenades. Ballist Res Lab Aberd Proving Ground MD 1943.
[35] M. Butterworth, M.R. Chassin, and R. McGrath, THE HYPOPHYSEAL GROWTH HORMONE, NATURE AND ACTIONS. Inter-national Symposium sponsored by the Henry Ford Hospital and Edsel B. Ford Institute for Medical Research, Detroit, Mich., and held at the Hospital October 27, 28, 29, 1954. Editors: Richmond W. Smith, Jr., MD, Oliver H. Gaebler, MD, and CNH Long, MD 576 pages, United States Armed Forces Medical Journal, vol. 6, no. 7-12, p. 1089, 1955.
[36] Ngo T, Mendis P, Gupta A, Ramsay J. Blast loading and blast effects on structures–an overview. Electron J Struct Eng 2007;(1):76–91.
[37] Hyde D. User's Guide for Microcomputer Programs CONWEP and FUNPRO. Applications of TM 5-855-1: Fundamentals of Protective Design for Conventional Weapons. Vicksburg, MS, USA: USA Army Engineers Waterways Experimentation; 1988.
[38] Entezari A, Esmaili J. Investigation on the Stress Distribution and Flexural Strength of Structural Lightweight Aggregate Concrete. Concr Res 2010;3:61–72.
[39] Lubliner J, Oliver J, Oller S, Oñate E. A plastic-damage model for concrete. Int J Solids Struct 1989;25(3):299–326.
[40] Jeeho L, Gregory L. Plastic-damage model for cyclic loading of concrete structures. J Eng Mech 1998;124(8):892–900.
[41] Yu T, Teng JG, Wong YL, Dong SL. Finite element modeling of confined concrete-II: Plastic-damage model. Eng Struct 2010;32(3):680–91.
[42] Lu J, Chen J, Zhu K, Xu H, Zhang W, Deng Q. Experimental and numerical studies on the behaviors of autoclaved aerated concrete panels with insulation boards subjected to wind loading. Materials 2021;14(24):7651.
[43] Lourenço PJBB. Computational strategies for masonry structures. PhD thesis, Delft University of Technology; 1997.
[44] Hamra, Lotfi. Development and analysis of low-order models of frame structures under blast loads. (2016). PhD thesis, Universite de Liege (Belgium).
[45] U.S. Department of Defense (DOD). Structures to Resist the Effects of Accidental Explosions (UFC 3-340-02); DOD: Washington, DC, USA, 2008.
[46] Masonry Standards Joint Committee (MSJC). Building Code Requirements and Specification for Masonry Structures: Containing Building Code Requirements for Masonry Structures (TMS 402-11/ACI 530-11/ASCE 5-11), and Specification for Masonry Structures TMS 402-11/ACI 530-11/ASCE 6-11), and Companion Commentaries; ASCE: Reston, VA, USA, 2016.
[47] Michelini E, Ferretti D, Miccoli L, Parisi F. Autoclaved aerated concrete masonry for energy efficient buildings: State of the art and future developments. Constr Build Mater 2023;402:132996.
[48] Wu T, Wei H, Liu X, Xing G. Factors Influ Mech Prop Lightweight Aggreg Concr 2017.
[49] K. Sherin and J. Saurabh, Review of autoclaved aerated concrete:-advantages and disadvantages, in *Proc. Natl. Conf. Adv. Struct. Mater. Methodol. Civ. Eng. (ASMMCE–2018)*, 2018, pp. 35-39.
[50] He X, Zheng Z, Yang J, Su Y, Wang T, Strnadel B. Feasibility of incorporating autoclaved aerated concrete waste for cement replacement in sustainable building materials. J Clean Prod 2020;250:119455.
[51] Zhou X, Hao H. Modelling of dynamic behaviour of brick masonry walls under blast loading. Int J Impact Eng 2008;35(5):363–75.
[52] Li C, Hao H, Wang Z. Dynamic properties of concrete material and structures under simulated blast loading. Int J Prot Struct 2006;1(1):1–20.
[53] BS EN 1991-1-7:2006 Eurocode 1 - Actions on structures. General actions - Accidental actions (+A1:2014) (incorporating corrigendum February 2010).
[54] The Steel Construction Institute. SCI P244: Protection of Buildings Against Explosions. Ascot, UK: The Steel Construction Institute; 2003.